Electronic Supplementary Information

Surface/interface engineering N-doped carbon/NiS_2 nanosheets for efficiently electrocatalytic H_2O splitting

Deliang Zhang[a, c]# and Hongyu Mou[b]#, Lei Chen,[a] Xing Gao,[c] Debao Wang,*[a] and Caixia Song*[b]

[a] Key Laboratory of Optic-electric Sensing and Analytical Chemistry for Life Science (MOE), and College of Chemistry and Molecular Engineering, Qingdao University of Science and Technology, Qingdao 266042, P. R. China, E-mail: dbwang@qust.edu.cn

[b] College of Materials Science and Engineering, Qingdao University of Science & Technology, Qingdao 266042, China

[c] School of Chemical and Biological Engineering, Qilu Institute of Technology, Jinan, 250200, P.R. China

# These authors contributed equally to this work.

Table of the contents

1. Experiment Section

Electrochemical measurements.

The catalyst dispersion mixture was prepared by adding a certain amount of catalysts with deionized water, ethanol and 5 wt.% Nafion solution under ultrasound. For the fabrication of working electrode, the as-obtained catalyst mixture was dropped coating onto a piece of carbon cloth (1 cm ×1 cm) and dried. The actual mass loading of active materials was 2.4 $mg \cdot cm^{-2}$. The electrochemical measurements were performed in 1 $mol \cdot L^{-1}$ KOH solution at room temperature in a standard three-electrode system and all the data was recorded by an electrochemical workstation (PARSTAT 3000). Graphite rod and Ag/AgCl electrode were used as a counter and a reference electrode, respectively. The measured potentials have been converted to reversible hydrogen evolution (RHE) following on the Nernst equation: $E_{RHE} = E_{Ag/AgCl} + 0.197 + 0.0591pH$. The electrocatalytic activities of all the electrodes were assessed using linear sweep voltammetry (LSV) at 5 $mV \cdot s^{-1}$. For ECSA measurement, cyclic voltammetry (CV) curves at different scan rates from 20 to 100 $mV \cdot s^{-1}$ in the range of 100-300 mV vs. RHE were conducted. A 90 % iR compensation was applied to all LSV polarization curves.

Characterization of the electrocatalyst.

XRD patterns of all the samples were collected using a powder X-ray diffractometer (D/max-2500/PC). SEM photographs were recorded with a Hitachi SU8010 field emission scanning electron microscope. A JEM-F200 transmission electron microscope has been applied to obtain TEM, HRTEM, and STEM micrographs and the correspondence elemental mapping An ESCALAB MK X-ray photoelectron spectra (XPS) have been recorded and applied to identify the surface composition and chemical states of the as-obtained samples. Raman spectra of the catalyst were recorded on a Labram HR800 laser micro confocal Raman spectrometer (HORIBA Jobin Yvon, excitation source: 532 nm YAG laser). AFM analysis was performed on a Dimension Icon atomic force microscope.

2. Supplementary Figures and Discussion

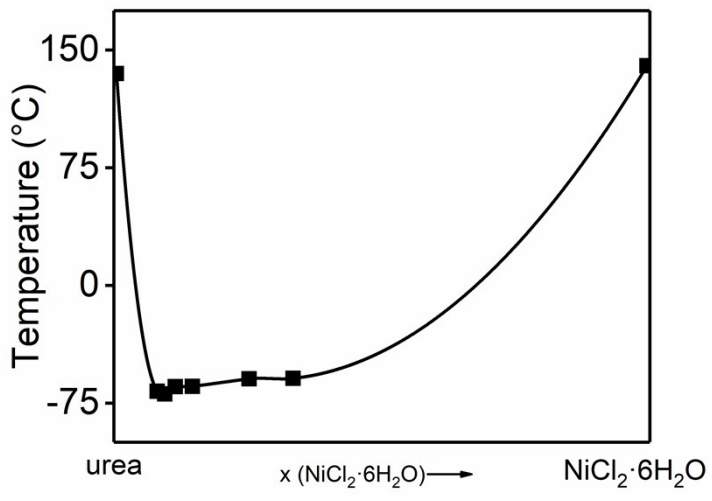

Figure S1. Phase diagram of DES composed of urea and $NiCl_2 \cdot 6H_2O$ at different molar ratio.

Differential scanning calorimetry (DSC) was performed using a Q2000 DSC system (TA Instruments-Waters LLC, USA) at a heating rate of 10 $^oC \cdot min^{-1}$. The melting points of urea (138 ^{o}C), $NiCl_2 \cdot 6H_2O$ (140 ^{o}C), and the $NiCl_2$-urea mixtures at different molar ratio were determined from DSC data. DSC curves proved that $NiCl_2$-urea mixture starts to melt from around -60.6 ^{o}C. This melting temperature is much lower than the melting point of urea (138 oC) and $NiCl_2 \cdot 6H_2O$ (140 ^{o}C), respectively, which demonstrates the formation of ionic liquid-like solution of $NiCl_2$-urea.

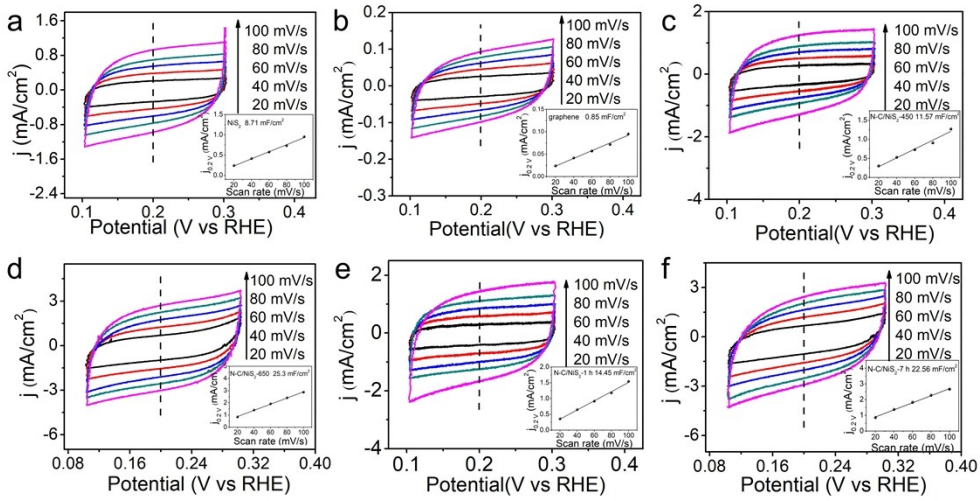

Figure S2. Cyclic voltammetry of (a) NiS_2, (b) graphene, (c) N-C/NiS_2-450 ^{o}C, (d) N-C/NiS_2-650 ^{o}C, (e) N-C/NiS_2-1 h, (f) N-C/NiS_2-7 h 0.10-0.30 V (vs. RHE) at different

scan rate.

Linear fitting of capacitive currents obtained at 0.2V vs the scan rate to acquire C_{dl}, and the corresponding of the samples values of C_{dl} are 8.71, 0.85, 11.57, 25.3, 14.45, and 22.56 mF cm^{-2}, respectively. The calculated ECSA of NiS_2, graphene carbon, and N-C/NiS_2 obtained with different reaction condition are 74, 7.3, 98.1, 214.4, 122.5, and 191.2 cm^2, respectively.

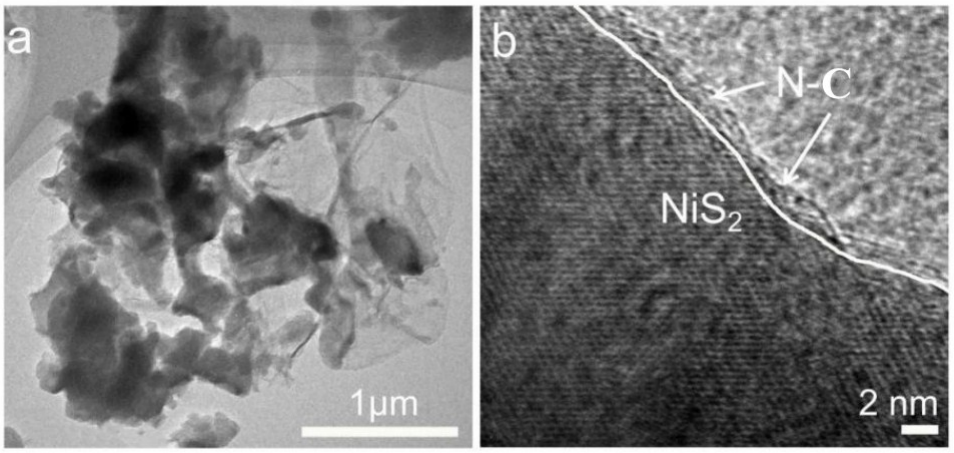

Figure S3. TEM and HRTEM images of N-C/NiS_2 catalyst after 48h HER stability experiments.

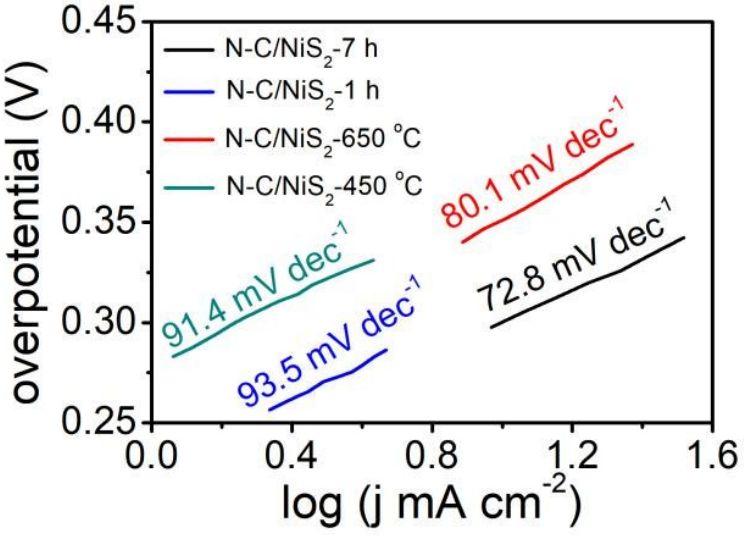

Figure S4. Tafel plots of different catalysts.

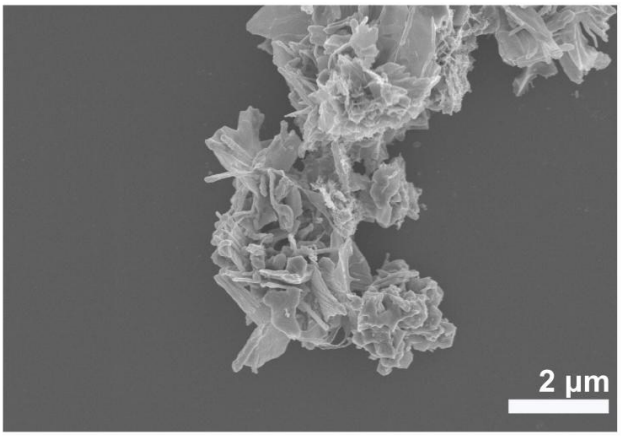

Figure S5. SEM image of N-C/NiS_2 after the OER stability test.

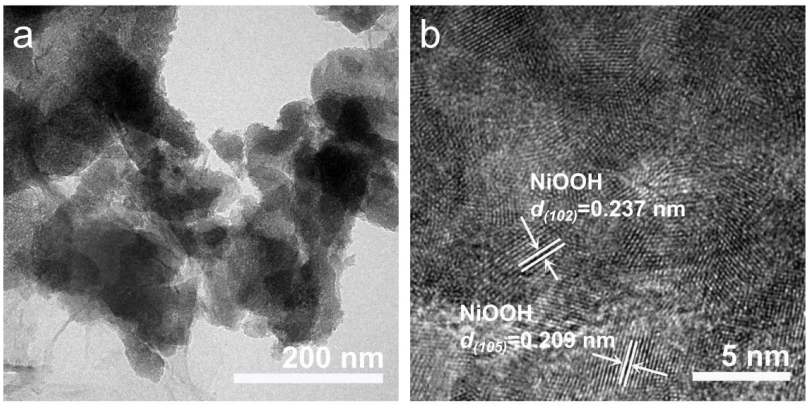

Figure S6. TEM and HRTEM images of N-C/NiS_2 after the OER stability test.

SEM, TEM, and HRTEM images in Fig. S5-6 show the structure evolution for the catalyst after OER stability test. The sheet-like morphology of N-C/NiS_2 (Fig. S5) maintains well, this phenomenon is also consistent with the TEM test results (Fig. S6a). Moreover, the corresponding HRTEM image is exhibited in Fig. S6b. The lattice distance of 0.209 nm and 0.237 nm further demonstrate the formation of NiOOH in the process of reaction which are designed for (105) and (102) facet of NiOOH (JCPDS# 06-0075).

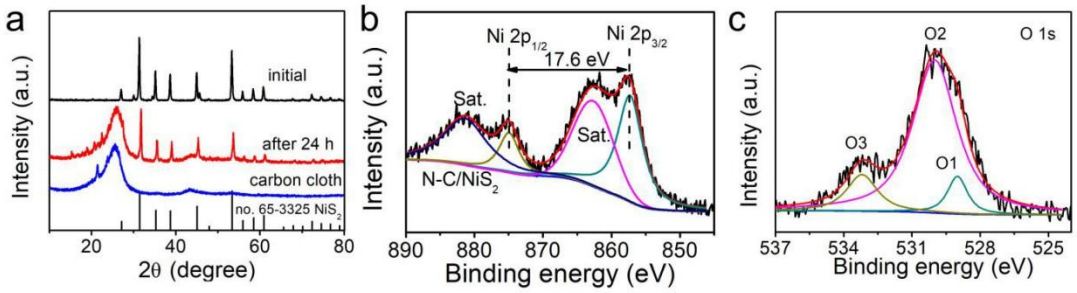

Figure S7. (a) XRD pattern of N-C/NiS_2, XPS spectra of N-C/NiS_2 (b) Ni 2p, (c) O

1s after the OER stability test.

The changes of chemical composition are further ascertained by XRD and XPS technique. As shown in Fig. S7a, the diffraction peaks of N-C/NiS_2 show no obvious change, indicating that the catalyst retains the same phase composition before and after the OER stability test. As for Ni 2p in Figure S7b, the energy separation of 17.6 eV demonstrate the presence of Ni^{3+}.[1] In other word, it suggests that the surface Ni^{2+} was oxidized after continuous electrochemical tests. While for O 1s after OER stability test, metal-O band (O1) appears in addition to hydroxyl group (O2) and the surface adsorbed oxygen species (O3) (Fig. S7c).

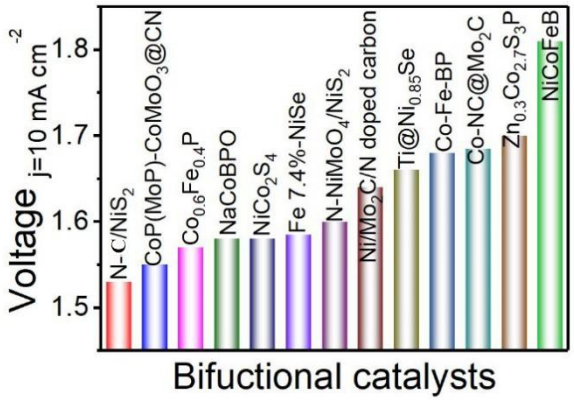

Figure S8. Comparison of voltage with other reported bifunctional catalysts at 10 $mA \cdot cm^{-2}$.[2-13]

3. Supplementary Tables

Table S1. Compare the HER performance of N-C/NiS_2 with other reported non-precious HER electrocatalysts.

Catalysts	η_{10} (mV)	Tafe Slope (mV dec^{-1})	electrolyte	Ref.
N-C/NiS_2	**78**	**63.4**	**1 M KOH**	**this work**
$(Fe_xNi_{1-x})_2P$	103	76.6	1 M KOH	*Nano energy*, 2019, **56**, 813.
$Co(OH)_x$@CoP	180	76	1 M KOH	*Chem. Sci.*, 2019, **10**, 2019.
Co_3O_4/MoS_2	205	98	1 M KOH	*Appl. Catal.*, B, 2019, **248**, 202.
Co-Fe-P	86	66	1 M KOH	*Nano energy*, 2019, **56**, 225.
CoNiP	145.8	52	1 M KOH	*J. Mater. Chem. A*, 2019, **7**, 8602.
$FePSe_3$-N-carbon	118.5	106	1 M KOH	*Nano Energy*, 2019, **57**, 222.
Mo_2C/Mo_2N	145	55	1 M KOH	*Adv. Funct. Mater*, 2019, **29**, 1807419.
MoO_3	138	50	1 M KOH	*J. Mater. Chem. A*, 2019, **7**, 257.
MoS_2/TiO_2	700	60	1 M KOH	*ACS Appl. Energy Mater.*, 2019, **2**, 2053.
NiCoN/C	103	-	1 M KOH	*Adv. Mater.*, 2019, **31**, 1805541.
Ni–N–C	147	114	1 M KOH	*Energy Environ. Sci.*, 2019, **12**, 149.
NiO/Ni	192	110	1 M NaOH	*Appl. Catal. B: Environ.*, 2019, **245**, 122.
S doped MoS_2	250	53	0.5M H_2SO_4	*Nanoscale Adv.*, 2019, **1**, 1489.
Co N doped graphene	230	99	0.5 M H_2SO_4	*Adv. Energy Mater.*, 2019, 9, 1803689.
1T-MoS_2	103	49	0.5 M H_2SO_4	*Small*, 2019, **15**, 1804903.
Co-WS_2	160	76	0.5 M H_2SO_4	*Sci. Rep.*, 2019, **9**, 1357.
MoS_2/rGO	154	77	0.5 M H_2SO_4	*Chem. Commun.*, 2019, **55**, 2078.
Ni@NC@MoS_2	82	47.5	0.5 M H_2SO_4	*Small*, 2019, **15**, 1804545.

Table S2. Compare the OER performance of N-C/NiS_2 with other reported non-precious OER electrocatalysts in KOH electrolyte.

Catalysts	η_{10} (mV)	Tafe Slope (mV dec^{-1})	KOH electrolyte	References
N-C/NiS_2	**264**	**51.3**	**1 M**	**this work**
$NiS_{1.03}$	270	68.9	1 M	*Small*, 2018, **14**, 1703273.
NiCoS/$Ti_3C_2T_x$	365	58.2	1 M	*ACS Appl. Mater. Interfaces*, 2018, **10**, 22311.
$FeNi_2S_4$	273	66	1 M	*J. Mater. Chem. A*, 2018, **6**, 19417
$Co_xNi_{1-x}S_2$	290	46	1 M	*J. Mater. Chem. A*, 2019, **7**, 3592
NGO/Ni_7S_6	380	45	0.1 M	*Adv. Funct. Mater.*, 2017, **27**, 1700451
$Co_2(OH)_3Cl$	270	155	1 M	*Adv. Mater.,* 2019, **31**, 1805127.
$Bi_7Fe_3Ti_3O_{21}$	470	87	1 M	*J. Am. Chem. Soc.*, 2019, **141**, 3121
Co(O)OH	322	-	1 M	*Angew. Chem. Int. Ed.*, 2019, **131**, 3529
Co-Fe-N	266	30	1 M	*Nano Energy*, 2019, **57**, 644
Co-graphdiyne	270	99	1 M	*J. Mater. Chem. A*, 2019, **7**, 5575.
Ni-BDC/$Ni(OH)_2$	320	41	1 M	*Nanoscale*, 2019, **11**, 3599.
Ni-Doped CuS	390	96.8	1 M	*Catal. Sci. Technol.*, 2019, **9**, 406.
$Ni_xFe_{1-x}O_yH_z$	290	28	1 M	*Angew. Chem. Int. Ed.*, 2019, **58**, 3769.
N+/NiO	400	136	0.1 M	*J. Mater. Chem. A*, 2019, **7**, 4729.

4. References

[1] L. Hou, Y. Shi, C. Wu, Y. Zhang, Y. Ma, X. Sun, J. Sun, X. Zhang and C. Yuan, *Adv. Funct. Mater.*, 2018, **28**, 1705921.

[2] C. Luan, J. Yang, H. Qiao, X. Dai, Y. Yang, and H. Zhao, *ACS Appl. Mater. Interfaces*, 2019, **11**, 76890-6899.

[3] Y. Lian, H. Sun, X. Wang, P. Qi, Q. Mu, Y. Chen, J. Ye, X. Zhao, Z. Deng and Y. Peng, *Chem. Sci.*, 2019, **10**, 464-474.

[4] P. Menezes, A. Indra, I. Zaharieva, C. Walter, S. Loos, S. Hoffmann, R. Schlögl, H. Dau and M. Driess, *Energy Environ. Sci.*, 2019, **12**, 988-999.

[5] Z. Kang, H. Guo, J. Wu, X. Sun, Z. Zhang, Q. Liao, S. Zhang, H. Si, P. Wu, L. Wang and Y. Zhang, *Adv. Funct. Mater.*, 2019, **29**, 1807031.

[6] Z. Zou, X. Wang, J. Huang, Z. Wu and F. Gao, *J. Mater. Chem. A*, 2019, **7**, 2233-2241.

[7] L. An, J. Feng, Y. Zhang, R. Wang, H. Liu, G. Wang, F. Cheng and P. Xi, *Adv. Funct. Mater.*, 2019, **29**, 1805298.

[8] M. Li, Y. Zhu, H. Wang, C. Wang, N. Pinna and X. Lu, *Adv. Energy Mater.*, 2019, **9**, 1803185.

[9] C. Yang, J. Zhang, G. Gao, D. Liu, R. Liu, R. Fan, S. Gan, Y. Wang and Y. Wang, *ChemSusChem*, 2019, **12**, 2271-2277.

[10] Z. Wu, D. Nie, M. Song, T. Jiao, G. Fu, and X. Liu, *Nanoscale*, 2019, **11**, 7506-7512.

[11] Q. Liang, H. Jin, Z. Wang, Y. Xiong, S. Yuan, X. Zeng, D. He and S. Mu, *Nano Energy*, 2019, **57**, 746-752.

[12] Z. Liang, Z. Yang, J. Dang, J. Qi, H. Yuan, J. Gao, W. Zhang, H. Zheng and R. Cao, *Chem. Eur. J.*, 2019, **25**, 621-626.

[13] Y. J. Li, B. Huang, Y. Sun, M. Luo, Y. Yang, Y. Qin, L. Wang, C. Li, F. Lv, W. Zhang and S. Guo, *Small*, 2019, **15**, 1804212.